



Article

# Dynamics Contributions to the Growth Mechanism of Ga<sub>2</sub>O<sub>3</sub> Thin Film and NWs Enabled by Ag Catalyst

Badriyah Alhalaili <sup>1,2,\*</sup> , Ryan Bunk <sup>2</sup>, Ruxandra Vidu <sup>2,3</sup> and M. Saif Islam <sup>2</sup>

<sup>1</sup> Nanotechnology and Advanced Materials Program, Kuwait Institute for Scientific Research, Safat 13109, Kuwait

<sup>2</sup> Electrical and Computer Engineering, University of California, Davis, CA 95616, USA; rjbunk@ucdavis.edu (R.B.); ruxiev@gmail.com (R.V.); sislam@ucdavis.edu (M.S.I.)

<sup>3</sup> The Faculty of Materials Science and Engineering, University of Politehnica of Bucharest, 060042 Bucharest, Romania

\* Correspondence: bhalaili@kisr.edu.kw or eng.kisr@hotmail.com

Received: 16 August 2019; Accepted: 3 September 2019; Published: 6 September 2019



**Abstract:** In the last few years, interest in the use of gallium oxide (Ga<sub>2</sub>O<sub>3</sub>) as a semiconductor for high power/high temperature devices and UV nano-sensors has grown. Ga<sub>2</sub>O<sub>3</sub> has an enormous band gap of 4.8 eV, which makes it well suited for applications in harsh environments. In this work, we explored the effect of Ag thin film as a catalyst to grow gallium oxide. The growth of gallium oxide thin film and nanowires can be achieved by heating and oxidizing pure gallium at high temperatures (~1000 °C) in the presence of trace amounts of oxygen. We present the results of structural, morphological, and elemental characterization of the β-Ga<sub>2</sub>O<sub>3</sub> thin film and nanowires. In addition, we explore and compare the sensing properties of the β-Ga<sub>2</sub>O<sub>3</sub> thin film and nanowires for UV detection. The proposed process can be optimized to a high scale production Ga<sub>2</sub>O<sub>3</sub> nanocrystalline thin film and nanowires. By using Ag thin film as a catalyst, we can control the growth parameters to obtain either nanocrystalline thin film or nanowires.

**Keywords:** thin film; nanowires; Ga<sub>2</sub>O<sub>3</sub>; quartz; thermal oxidation; silver catalyst

## 1. Introduction

In recent years, gallium oxide (Ga<sub>2</sub>O<sub>3</sub>) has become one of the most significant materials that can operate in harsh conditions such as automobiles engines, flame monitoring, space communications, and detection of missiles. This material has a band-gap of 4.8 eV, a high melting point of 1900 °C, and excellent electrical and photoluminescence properties [1–3]. Ga<sub>2</sub>O<sub>3</sub> has the potential to replace Si, SiC, GaN/AlGaN in high power applications due to its superior breakdown voltage and low on-resistance [4]. Additionally, the fundamental band gap is above the upper range of the terrestrial solar spectrum; hence, Ga<sub>2</sub>O<sub>3</sub> is expected to be intrinsically solar-blind as a photodetector [5,6]. Therefore, it is considered the best choice for visible-blind (UV) photodetectors and power electronics in harsh environments.

Although Ga<sub>2</sub>O<sub>3</sub> is a desired material in the semiconductor industry, the cost of Ga<sub>2</sub>O<sub>3</sub> wafers is still prohibitively high and methods for the top-down and bottom-up fabrication of Ga<sub>2</sub>O<sub>3</sub> nanostructures are still immature. Hence, a wide variety of methods to grow Ga<sub>2</sub>O<sub>3</sub> thin film and nanowires have been explored, such as thermal oxidation [7,8], vapor–liquid–solid growth [9], pulsed laser deposition [10], sputtering [11], thermal evaporation [12–14], molecular beam epitaxy [15], laser ablation [16], arc-discharge [17], carbothermal reduction [18], microwave plasma [19], metalorganic chemical vapor deposition [20], and the hydrothermal method [21,22]. In this work, the thermal oxidation process was performed to explore the effect of silver thin film as a catalyst to enhance

the growth of Ga<sub>2</sub>O<sub>3</sub>. This process is one of the less expensive techniques that operate at a high temperature. In addition, Ag helps to increase the growth of Ga<sub>2</sub>O<sub>3</sub> due to the self-assembly growth of nanocrystalline grains [23]. Consequently, the presence of an effective catalyst that has the ability to tolerate higher temperatures than its melting point could be a valuable factor in spontaneously increasing the reaction rate of the growth mechanism.

Silver nanoparticles (Ag NPs) have been explored as a possible catalyst for Ga<sub>2</sub>O<sub>3</sub> nanowire growth [9,24,25]. In addition, silver has been used as a photocatalyst and doping material for different materials such as MoS<sub>2</sub>, SnO<sub>2</sub> nanostructures, and TiO<sub>2</sub>/SnO<sub>2</sub> nanocomposite [26–28]. To date, the effect of Ag thin film as a catalyst on Ga<sub>2</sub>O<sub>3</sub> growth of thin film and nanowire at different growth parameters have not been explored. Because of oxygen's high diffusivity and solubility at higher temperatures, more atmospheric O<sub>2</sub> accumulation leads to effective transport into the Ga and enhance spontaneous Ga<sub>2</sub>O<sub>3</sub> growth. However, other metals used as catalysts either lack solubility (Au) or diffusivity (Fe).

We propose a simple and inexpensive thermal oxidation process to produce Ga<sub>2</sub>O<sub>3</sub> thin film and nanowires using 5 nm and 300 nm Ag thin film as a catalyst patterned on a quartz substrate. Because the influence of the oxidation parameters (i.e., annealing temperature, time, and oxygen concentration) and Ag film thickness on Ga<sub>2</sub>O<sub>3</sub> growth had not been comprehensively investigated, various parameters of Ga<sub>2</sub>O<sub>3</sub> growth due to silver presence were examined in this work. Different characterization techniques, such as X-ray diffraction (XRD), scanning electron microscopy (SEM), energy dispersive X-ray spectroscopy (EDS), and electrical measurements have been performed in this study to explore the growth mechanism of thin film and nanowire of Ga<sub>2</sub>O<sub>3</sub>.

## 2. Materials and Methods

Quartz substrates used in this experiment were 500 μm thick and 15 mm in diameter. First, quartz substrates were cleaned with acetone and ethyl alcohol, rinsed with deionized water, and then dried with an N<sub>2</sub> blow gun to remove the excess residues. To investigate the effect of Ag NPs during the growth of Ga<sub>2</sub>O<sub>3</sub>, two different thicknesses of Ag thin film such as 5 nm and 300 nm were deposited on the samples with a Lesker sputtering system by using a shadow mask. This patterned surface offers the opportunity to investigate concomitantly the growth of gallium oxide on Ag-coated and uncoated surfaces. We have also compared the results with uncoated samples grown under the same conditions.

Then, the sample was loaded into a quartz crucible which was placed into an OTF-1200X-50-SL horizontal alumina tube furnace made by MTI Corporation (MTI Corporation, Richmond, CA, USA). A controlled stream of O<sub>2</sub> and N<sub>2</sub> mixture gases flowing through the quartz tube was performed to trace the concentration of oxygen molecules by using an oxygen analyzer (EQ-W1000-LD, MTI Corporation, Richmond, CA, USA) made by MTI Corporation. The samples were heated up to 1000 °C for 60 min, with a controlled heating and cooling rate of 17 °C per second. The temperature was regulated during heating, cooling, and holding by use of a proportional-integral-derivative (PID) controller. The entire process occurred in a flow of 20 sccm nitrogen atmosphere. The concentration of O<sub>2</sub> gas was varied by adjusting the gas flow controller, which controlled the ratio of O<sub>2</sub> to N<sub>2</sub> gas. The background oxygen concentration was determined to be from 88 ppm to 280 ppm. Samples were positioned so that the silver patterned surface faced the gallium pool. The distance between the substrate and the gallium pool was 10 mm. Then, the quartz crucible was inserted inside the furnace for the oxidation process. Figure 1 illustrates the set-up of the sample inside the furnace, which was used to grow gallium oxide on an Ag catalyst patterned surface.

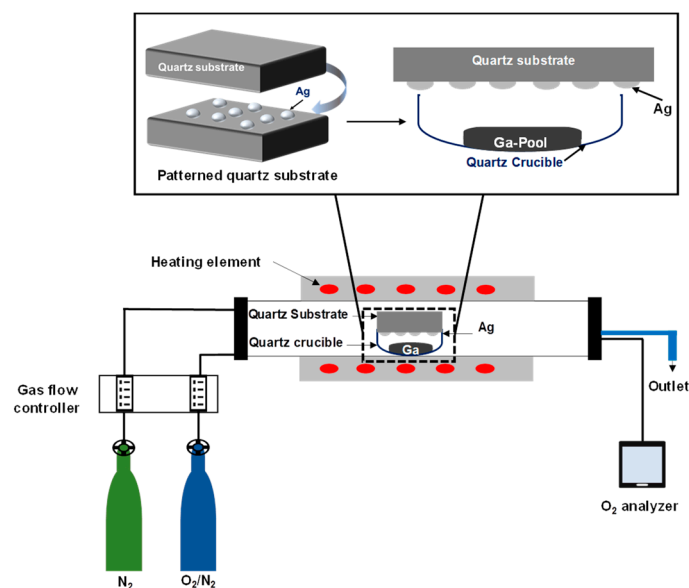


**Figure 1.** Schematic of the sample set-up inside the furnace, which was used to study the growth mechanism of gallium oxide on a quartz substrate coated with a 5 nm and 300 nm patterned Ag film sputtered by a shadow mask. The quartz substrate was placed over the Ga source, having the patterned surface facing downward over the Ga source. The Ga liquid pool is in a quartz crucible at a distance of ~10 mm from the sample.

### 3. Results & Discussion

#### 3.1. X-ray Diffraction

X-ray Diffraction was performed with a Panalytical XPert PRO Diffractometer (Malvern Panalytical, Netherlands). Figure 2 shows the peak positions of the X-ray diffraction pattern of grown  $\text{Ga}_2\text{O}_3$  on quartz substrates oxidized at 1000 °C from the main planes in the crystalline  $\beta\text{-Ga}_2\text{O}_3$ . The results are consistent with polycrystalline  $\beta\text{-Ga}_2\text{O}_3$  as referenced against International Center for Diffraction Data (ICDD) standard PDF 00-041-1103 [29]. All major peaks of the  $\beta\text{-Ga}_2\text{O}_3$  phase are seen to be present in the diffraction data, which strongly indicates the presence of  $\beta\text{-Ga}_2\text{O}_3$ .

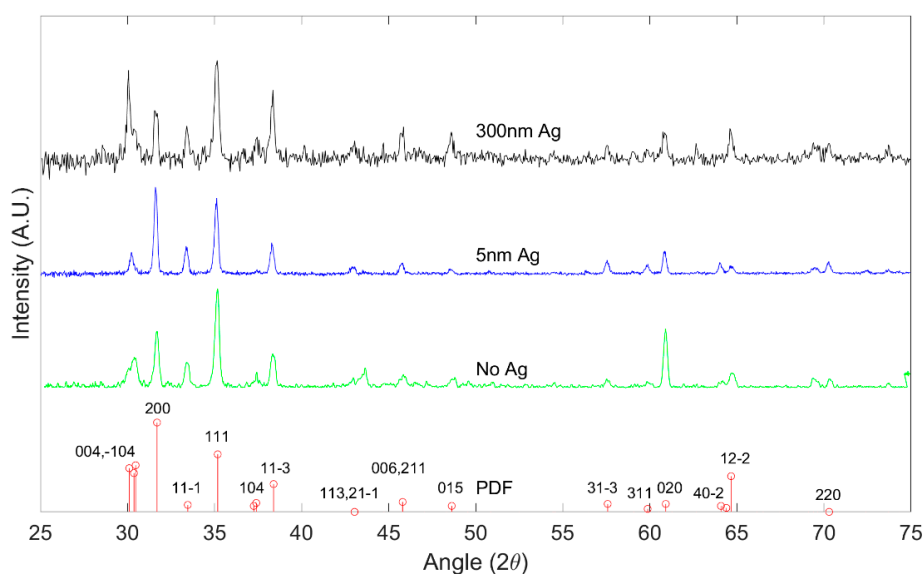


**Figure 2.** X-ray diffraction (XRD) pattern of  $\beta\text{-Ga}_2\text{O}_3$  for different Ag thickness at 1000 °C, indexed in comparison to PDF 00-041-1103.

### 3.2. SEM Characterization

The morphology of  $\text{Ga}_2\text{O}_3$  nanowires and thin films that were concomitantly grown on Ag-patterned quartz at  $1000^\circ\text{C}$  is shown in Figure 3. The Ag-patterned quartz surface shows distinct nanowires and thin film morphologies of  $\text{Ga}_2\text{O}_3$  that were grown concurrently on Ag-coated and uncoated areas, as illustrated in Figure 3. Ag-patterned areas have been converted into dense nanowires while the uncoated areas became a nonuniform coating of  $\text{Ga}_2\text{O}_3$  thin film. In the Ag-patterned areas, the nanowire density was increased, and their diameter was reduced depending on the Ag thin film thickness. The diameter of Ag-free growth was about 150–270 nm. When 5 nm and 300 nm Ag thin film was used, the NWs diameters were 120–160 and 80–130 nm, respectively. Even though the sample coated with 300 nm Ag has reduced the diameter of the nanowire and increase its density (Figure 4), we consider that presenting the sample coated with 300 nm Ag does not bring anything new. Hence, the results obtained for 5 nm Ag are further discussed and compared to the 300 nm Ag.

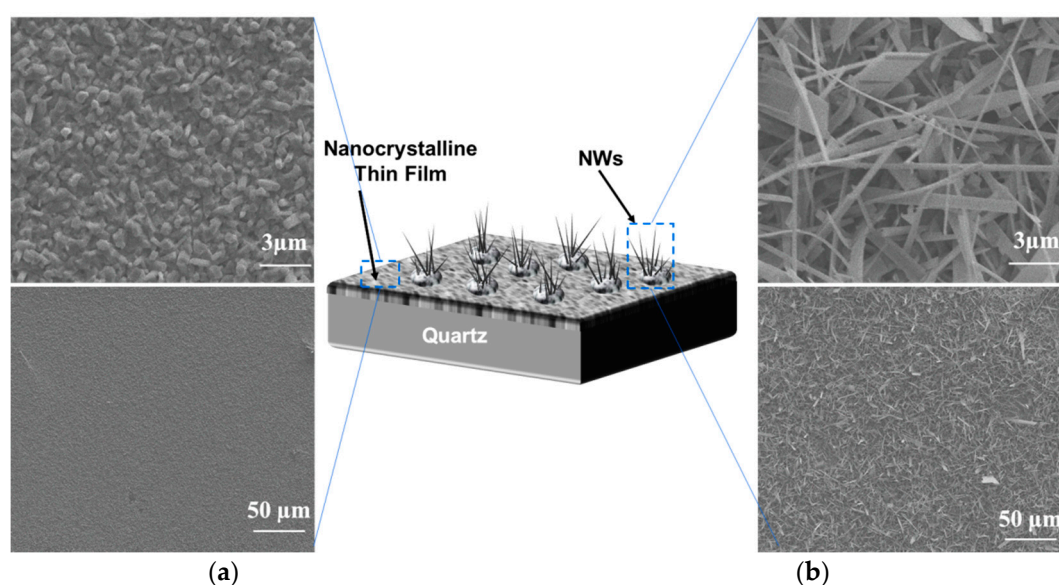


**Figure 3.** Scanning electron microscopy (SEM) images of 5 nm Ag-coated and uncoated areas acquired in the regions indicated in the illustration (middle). (a) Thin film. (b) nanowires.

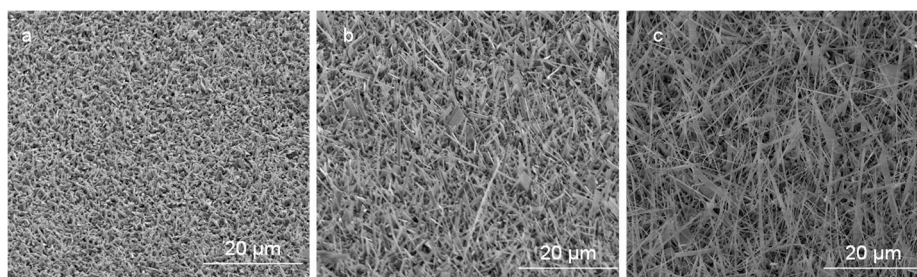


**Figure 4.** SEM images of uncoated and Ag-coated areas acquired in the regions indicated in the illustration. (a) nanocrystalline thin film of  $\text{Ga}_2\text{O}_3$  obtained by the indirect effect of the sample patterned by Ag catalyst within the uncoated area. (b)  $\text{Ga}_2\text{O}_3$  NWs under the presence of 5 nm Ag. (c)  $\text{Ga}_2\text{O}_3$  NWs under the presence of 300 nm Ag.

Figure 5 shows SEM images of the 5 nm Ag patterned quartz circles, which were converted into dense and long  $\text{Ga}_2\text{O}_3$  nanowires; however, the bare quartz was converted into  $\text{Ga}_2\text{O}_3$  nanocrystalline thin film. The area between Ag circles and the uncoated surface shows a gradual morphology from nanowires to thin film due to the lateral diffusion of Ag atoms. The lateral diffusion and distribution

of Ag enhance the growth of nanowires and increase the process rapidly and spontaneously in the area that was intentionally coated with Ag thin film. In addition, the presence of Ag affects the uncoated area and enhances nucleation of nanocrystalline thin film of  $\text{Ga}_2\text{O}_3$ . Due to the self-diffusion of Ag atoms, more oxygen molecules will enhance the dissolution of gallium suboxide ( $\text{Ga}_2\text{O}$ ) in the liquid Ag and deposit Gallium (III) oxide ( $\text{Ga}_2\text{O}_3$ ) through crystal nucleation on the bare quartz by vapor–liquid–solid (VLS) growth mechanism to form a nanocrystalline thin film [9].

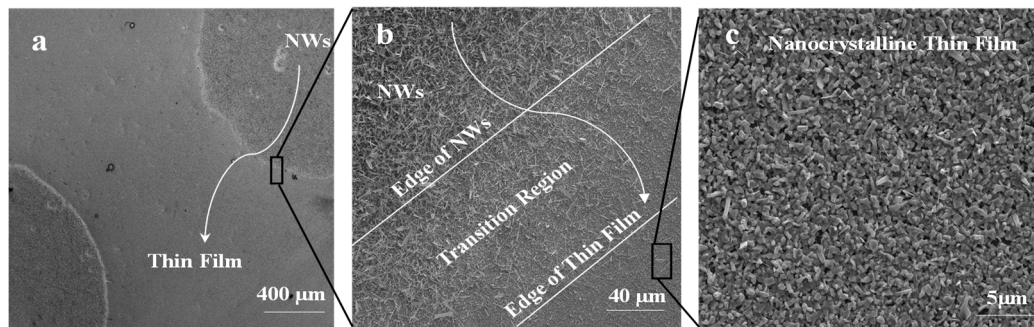


**Figure 5.**  $\text{Ga}_2\text{O}_3$  NWs grown on quartz at 1000 °C. (a) Top view of Ag circle pattern which was converted into dense NWs and surrounded by a nonuniform coating of thin film. (b) Interface of Ag-coated area and uncoated region shows a gradual transition of NW growth to thin film. (c) Nanocrystalline thin film of  $\text{Ga}_2\text{O}_3$  is due to surface diffusion of silver nanoparticles (Ag NPs).

Different types of self-diffusion can affect the distribution of Ag atoms on the surface. Surface diffusion has the lowest activation energy (0.39 eV) compared to the activation energy of grain boundary diffusion (0.99 eV) and volume diffusion (1.98 eV) [30]. Therefore, during the surface diffusion process, Ag atoms can move easily with no restriction and spread on the surface. At a low activation energy and high diffusion rate, the flux of atoms increases as the concentration gradient and temperature increase. It has been observed that as the temperature increases, the density of Ag nanoparticles also increases [31]. However, grain boundary diffusion and surface diffusion are predictable mechanisms in the oxidation process. Surface diffusion increases as the duration of thermal annealing increases within a fixed temperature [32,33].

### 3.3. FIB/EDS Characterization

A focused ion beam (FIB) equipped with X-MaxN 50 mm<sup>2</sup> energy dispersive spectroscopy (EDS) from Oxford Instruments was used to perform elemental and chemical microanalyses on the samples. EDS mapping results of oxidized Ga without and with 5 nm Ag catalyst at 1000 °C for 60 min are presented in Figure 6. It is obvious that the atomic percentage of Ga was almost doubled under the presence of Ag catalyst. Due to the EDS detection limit, the presence of Ag atoms was not detected even though the morphology of grown  $\text{Ga}_2\text{O}_3$  on Ag was greatly influenced compare to the Ag-free  $\text{Ga}_2\text{O}_3$ . The growth of gallium oxide is based on the vapor–liquid–solid (VLS) process [9].  $\text{Ga}_2\text{O}$  vapor was used as the gas source and the Ag catalyst served as the active site, leading to the growth of solid  $\text{Ga}_2\text{O}_3$  at 1000 °C.

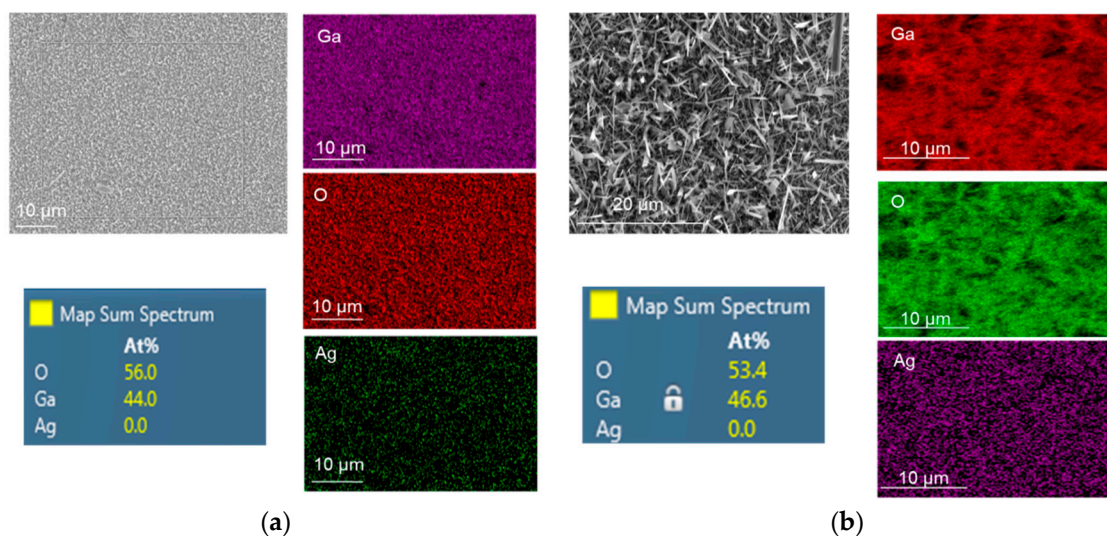


**Figure 6.** Energy dispersive spectroscopy (EDS) mapping of  $\text{Ga}_2\text{O}_3$  grown at  $1000\text{ }^\circ\text{C}$  on quartz surface: (a) Nanocrystalline film of  $\text{Ga}_2\text{O}_3$ . (b)  $\text{Ga}_2\text{O}_3$  nanowires catalyzed by 5 nm Ag. Longer and denser NWs were achieved when Ag was used as a catalyst.

### 3.4. Scanning Transmission Electron Microscopy (STEM)

Figure 7 shows a STEM image of the bright field (BF) and high-angle annular dark field (HAADF) of  $\text{Ga}_2\text{O}_3$  nanowire grown on the quartz coated with 5 nm Ag and oxidized at  $1000\text{ }^\circ\text{C}$ . The  $\beta\text{-Ga}_2\text{O}_3$  nanowire contained a few NPs with diameters between 5–10 nm that decorated the surface. The bright field showed dark NPs due to diffraction contrast since they are crystalline. Furthermore, HAADF was performed to capture z-contrast of Ag NPs. The NPs appear much brighter which suggest the average composition is heavier. Thus, the HAADF image of NPs has low noise and was expected to show a solid bright signal due to the high mass of the nanoparticles. This could suggest that these NPs could be Ag NPs.

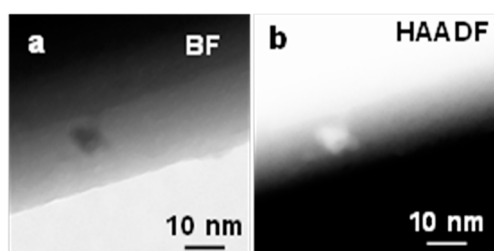


**Figure 7.** (a) Bright field (BF) (b) high-angle annular dark-field (HAADF) STEM images of Ag NPs at the interface of  $\text{Ga}_2\text{O}_3$  nanowire growth on quartz substrate at  $1000\text{ }^\circ\text{C}$ . The NP was bright due to z-contrast.

### 3.5. Factors Effecting the $\text{Ga}_2\text{O}_3$ Growth

- Silver Thin Film Thickness

Two different thicknesses of silver thin film have been selected to explore their morphological effects onto the growth kinetics under Ag presence, i.e., 5 nm and 300 nm, as shown in Figures 3b and 6b, respectively. Ag thin films could be an alternative catalyst technique to nanoparticles for  $\text{Ga}_2\text{O}_3$  growth since Ag plays a critical role in increasing the nanocrystalline nucleation of the film and forming denser, longer, and thinner nanowires as the temperatures increase above the silver melting point.

Obviously, the growth kinetics are highly influenced by the thickness of the Ag thin film and high oxidation temperatures. When Ag thin film was 5 nm, silver film dewets and forms nanoparticle-like

structures [34]. It has been shown that 5 nm and 10 nm Ag thin film dewets very fast at a temperature below 400 °C [34], leading to a fast conversion of Ag thin film to NPs. Consequently, this process could be more beneficial to form nanowires directly on the quartz substrate. However, as the thickness of Ag thin film increases (300 nm), the film requires a higher temperature (i.e.,  $T > 800$  °C) to shrink and form nanoparticles that enhance the growth of Ga<sub>2</sub>O<sub>3</sub> as shown in Figure 8. The formation of nanoparticle is more sluggish with thicker Ag films, as more time and temperature are required to complete the dewetting of the film. At a constant temperature (1000 °C), the formation of a thicker nanocrystalline layer of Ga<sub>2</sub>O<sub>3</sub> was increased at a shorter time and thinner and denser nanowires at a longer time.

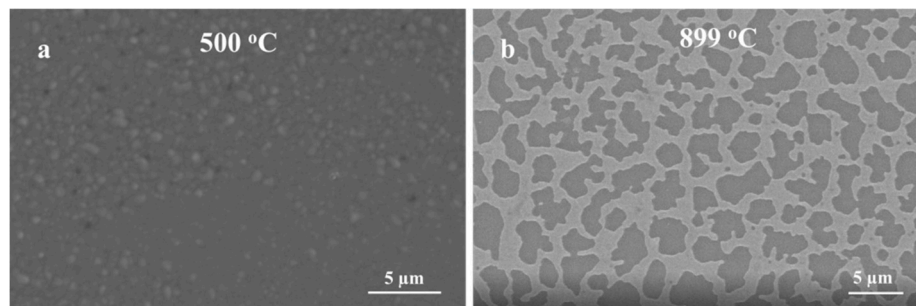


**Figure 8.** SEM images of the annealed Ag thin film of different thickness on quartz. (a) 5 nm Ag, (b) 300 nm Ag.

The method of annealing thin films was used in the past to generate metal nanoparticles that act as a catalyst for thin film or nanowire growth. Using this method, first, a silver thin film is deposited onto a substrate. When the substrate was heated, the thin film dewets forming silver nanoparticles (Ag NPs). The benefit of first using a thin film [35] instead of directly applying nanoparticles is that it maximizes the size and density of the nanoparticles.

- Oxidation Temperature

The Ga<sub>2</sub>O<sub>3</sub> nucleation and growth of nanowires and nanocrystalline thin film on Ag catalyst could be influenced by temperature. In order to assess the effect of the Ag catalyst, Ag on GaAs was oxidized at different temperatures to measure the effect of Ag's melting temperature (961.8 °C) on the growth of Ga<sub>2</sub>O<sub>3</sub> nanowires and thin film. The results show that temperature is the major factor that serves to enhance the Ga<sub>2</sub>O<sub>3</sub> growth mechanism due to the distribution of self-diffusion of Ag NPs, leading to increase the absorption of oxygen. The growth of Ga<sub>2</sub>O<sub>3</sub> nanowires at 800 °C and 1000 °C with constant oxygen supply and sputtering 300 nm Ag thin film at the surface of liquid gallium on quartz substrate showed a remarkable growth of Ga<sub>2</sub>O<sub>3</sub> nanowire for the first time via thermal oxidation (Figure 9). These results are in accordance with other reports [9,36] and it can be inferred that the impacts of the silver catalyst are related to the elevated temperatures. Figure 9 shows SEM images of Ga<sub>2</sub>O<sub>3</sub> growth in the presence of 300 nm silver at 800 °C and 1000 °C for 60 min. High accumulation of nanocrystalline grains and short nanowires at 800 °C with diameters and lengths in the range of 500 nm–1 μm were observed at 800 °C; however, longer, denser, and thinner nanowires were obtained at 1000 °C compared to 800 °C. The diameters of Ga<sub>2</sub>O<sub>3</sub> NWs are in the range of tens of nanometers and the length can reach several tens of micrometers, which mainly depend on the temperature and Ag catalyst.

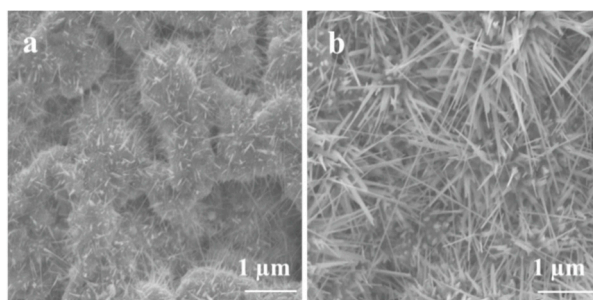


**Figure 9.** The effect of the oxidation temperature on the growth of  $\text{Ga}_2\text{O}_3$  in the presence of 300 nm Ag catalyst. (a) 800 °C. (b) 1000 °C.

First of all, high oxygen diffusion at a high temperature can be attained by using Ag catalyst which resulted in enhanced nanowire growth. The diffusion coefficient of oxygen in silver thin film shows that Ag is a better catalyst for enhancing the density and length of  $\text{Ga}_2\text{O}_3$  nanowires than other nanoparticle catalysts, such as Au [37–39], Fe [40], or Pt [41], due to its higher value, which means that silver has a higher tendency to absorb oxygen. Secondly, the solubility of oxygen in molten silver thin film can be increased by increasing its temperature above its melting point of 961.8 °C.

High temperatures could reduce the surface energy of Ag islands and increase the diffusion of Ag NPs due to the driving force at the surface. Increasing the droplet surface will increase oxygen adsorption and diffusion. In addition, it increases the mobility, agglomeration, and distribution of Ag NPs [31,42]. As a result, temperature has a great influence on the kinetics of the growth mechanism due to the physical properties of oxygen in Ag, such as its melting point, diffusivity, and solubility.

- Oxygen Concentration

The effect of oxygen flow rates on  $\text{Ga}_2\text{O}_3$  growth at a constant annealing temperature (1000 °C) and time (10 min) has been investigated. Figure 10 shows SEM images of nanocrystalline  $\text{Ga}_2\text{O}_3$  growth on quartz coated with 300 nm Ag thin film at 1000 °C and various oxygen concentrations and time. Obviously, the nucleation of nanocrystalline  $\text{Ga}_2\text{O}_3$  was increased as the oxygen concentration increased from 0.088 mL/min to 0.28 mL/min at constant time, leading to thicker coating of nanocrystalline  $\text{Ga}_2\text{O}_3$  on quartz substrate (Figure 10a,b). The growth of  $\text{Ga}_2\text{O}_3$  was accomplished under a very low oxygen flow rate. Then the number density became much higher when the flow rate increased to 0.16 mL/min. However, after additionally increasing the flow rate to 0.28 mL/min, the nanocrystalline growth was increased and the film was still showing large crystallites. As the oxygen concentration and time increased from 0.088 mL/min to 0.28 mL/min, the accumulation of grown nanocrystalline  $\text{Ga}_2\text{O}_3$  was slightly controlled, forming improved coating and growth of  $\text{Ga}_2\text{O}_3$  on the surface of the quartz (Figure 10a,c). From these results, it could be expected that  $\text{Ga}_2\text{O}_3$  requires more time to complete the growth from a nanocrystalline film in a short time (Figure 11) and that the nanowire nucleation will take longer (Figure 9b). Alternatively, these results may suggest that the nanowire growth observed at 300 nm silver films self-nucleates on the crystallites formed from a thick Ag film.

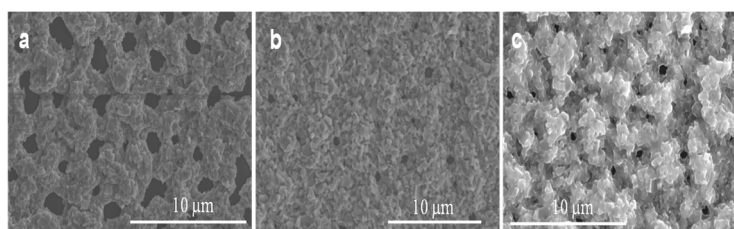


**Figure 10.** Growth of nanocrystalline grains of  $\text{Ga}_2\text{O}_3$  under 300 nm Ag presence at different oxygen concentrations. (a) 0.088 mL/min. (b) 0.16 mL/min. (c) 0.28 mL/min.

The grain size plays an important role in  $\text{Ga}_2\text{O}_3$  nanowire growth. Specifically,  $\text{Ga}_2\text{O}_3$  nanowires with much higher number density and aspect ratio (longer and thinner nanowires) were achieved from nanocrystalline  $\text{Ga}_2\text{O}_3$ . Besides, other factors such as surface morphology and shape of Ag catalyst may affect the nucleation and/or diffusion of  $\text{Ga}_2\text{O}_3$  nanocrystalline and nanowire growth. The catalyst sets the nucleation spot and drives the one-dimensionality of  $\text{Ga}_2\text{O}_3$  nanowire growth (Figures 3b and 9). Due to the difficulty to control these factors, other parameters such as temperature, time, atmosphere, and  $\text{Ga}_2\text{O}_3$  grain size are considered in the growth mechanism.

The influence of the oxidation atmosphere has significant impacts on the growth of nanowire due to the presence of Ag thin film. It has been observed that the motion of Ag NPs is influenced by the gas flow. The heated Ag films in the  $\text{N}_2$  gas dewet faster than the film in the Ar gas due to the molecular mass of  $\text{N}_2$  compared to Ar [34], leading to faster diffusion of Ag atoms. The higher mass of Ar limits diffusion through it, changing the growth dynamics. Furthermore, heating Ag NPs in an  $\text{O}_2$  gas as opposed to vacuum increases the surface self-diffusion of Ag atoms. Hence, the diffusion mechanism of Ag NPs enhances the growth of nanocrystalline thin film.

- Oxidation Time

To get a better understanding of the initial nucleation and growth of  $\text{Ga}_2\text{O}_3$  on the surface of the quartz, very short heating times were performed to observe the morphology and composition of the short-growth material. As seen in Figure 11, for a growth time of 5 min, the influence of 5 nm Ag thin film catalyst produces a dense forest-like film of short nanowire; however, the film appears to have a more compacted mixture of  $\text{Ga}_2\text{O}_3$  crystallites and silver at 300 nm Ag thin film. This result suggests that the nucleation and growth of  $\text{Ga}_2\text{O}_3$  at 300 nm Ag is more sluggish, as would be expected from the more difficult dewetting behavior of 300 nm Ag films. On the other hand, the 5 nm Ag film rapidly dewets and nucleates, producing dense nanowires that grow early in the oxidation process.

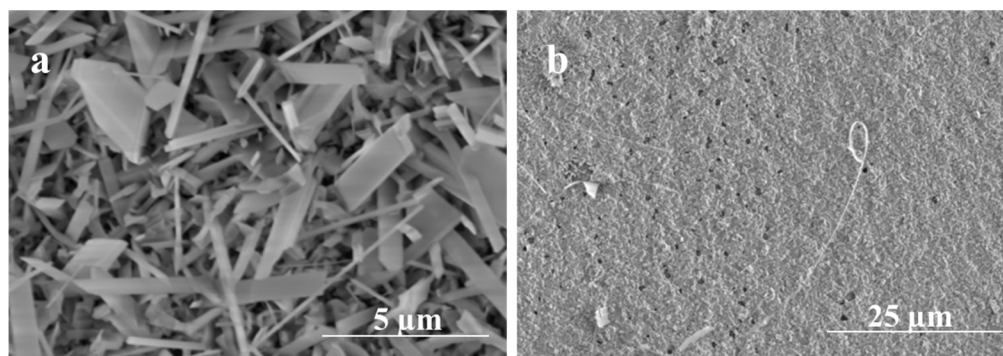


**Figure 11.** SEM images of  $\text{Ga}_2\text{O}_3$  obtained at 1000 °C for 5 min. (a) Denser growth of nanowires using 5 nm Ag. (b) Nanocrystalline grains growth using 300 nm Ag.

- Growth Mechanism

The use of a metal catalyst adds a new dynamic that contributes to enhancing the growth kinetics of  $\text{Ga}_2\text{O}_3$  nanostructures due to its simultaneous interactions with  $\text{O}_2$ , Ag, and the  $\text{Ga}_2\text{O}_3$  surface. The growth mechanism is summarized in Figure 12. In general, there is a lack of experimental results that discuss the chemical and physical interactions between Ga and O. However, it is well known that the solubility of oxygen in liquid Ga increases with increasing oxidation temperature [43]. At higher temperatures, Ga forms gallium suboxide vapor ( $\text{Ga}_2\text{O}$ ) in the presence of oxygen (Figure 12). This vapor dissociates into liquid Ga and  $\text{Ga}_2\text{O}_3$  on the Ag-patterned quartz surface. At temperatures above 200 °C,  $\text{Ag}_2\text{O}$  dissociates into Ag and  $\text{O}_2$ .

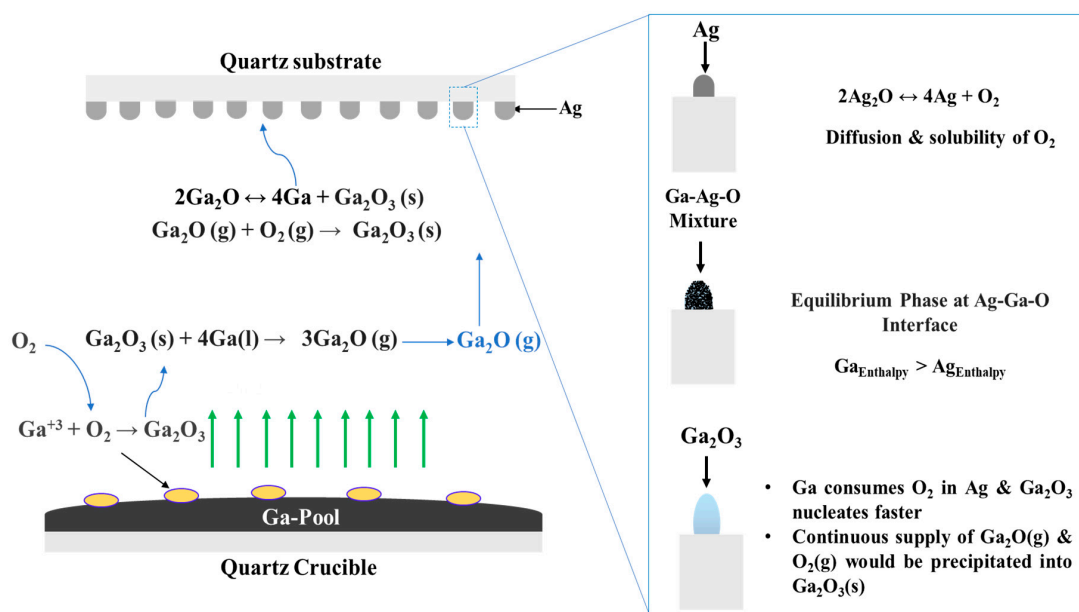


**Figure 12.** Schematic illustration of the proposed growth mechanism of  $\text{Ga}_2\text{O}_3$  on the Ag-patterned quartz surface.

There are many reasons that could explain the oxygen interaction at the O and Ag interface. First, the silver catalyst increases the rate of oxygen adsorption with increasing temperature [44]. Originally,  $\text{O}_2$  atoms are adsorbed in Ag catalyst to form surface atomic oxygen and desorbed as  $\text{O}_2$  or diffused by volume diffusion. At 1000 °C, as  $\text{O}_2$  diffusivity and solubility into Ag is increased, liquid Ga strips oxygen from Ag at the liquid interface of the molten Ga and Ag mixture. The adsorption of  $\text{O}_2$  in the presence of dissolved Ga leads to the formation of the solid  $\text{Ga}_2\text{O}_3$  surface. Eutectic reactions become possible with increasing temperature, and the interface changes from solid to a liquid–solid interface, which plays an important role in the supersaturation of the liquid–solid solution. The shape of the nanostructures is determined according to the nuclei surface formed on oxygenated gallium species [45] and Ag nanoparticles [46]. Different factors could determine the shape of the formed nanostructures such as pattern formation and time of coalescence, temperature, catalyst properties, etc. However, the degree of supersaturation is the dominant factor that controls the morphology of the growth.

- **Electrical Properties of the  $\text{Ga}_2\text{O}_3$  Film and Nanowires**

The electrical contact consisted of 10 nm Cr and 150 nm Au and was sputtered on the gallium oxide surface to measure the electrical conductivity and the photocurrent response of  $\beta\text{-Ga}_2\text{O}_3$  thin film and nanowires on quartz (Figure 13a). A custom probe station attached to a Keithly 2400 SMU was used with a UV light intensity of 15 W/cm<sup>2</sup>. The current–voltage (I–V) characteristics were measured at 10 V in dark conditions and under UV illumination (Figure 13b). Photocurrents were comparable to the dark current. The photoconductivity mechanism of the  $\beta\text{-Ga}_2\text{O}_3$  NWs is credited to surface oxygen adsorption and desorption process [47], which is highly influenced by the presence of silver as a catalyst, leading to improved oxygen detection and hence the electrical properties of the  $\beta\text{-Ga}_2\text{O}_3$  nanowires.

The photo-to-dark current ratio was much higher for the nanowires compared to the film. The photocurrent of nanowires was in the range of  $2.33 \times 10^{-7}$  A, which is one order of magnitude higher than that of thin film ( $9.16 \times 10^{-8}$  A). The trap states of oxygen generated at the surface of  $\text{Ga}_2\text{O}_3$  have a large impact on the photodetector performance [48]. Due to the large surface-to-volume ratio of nanowires and the existence of Ag NPs, the surface of NWs with trapped oxygen becomes highly sensitive. Nanowires as compared to thin films have a higher density of exposed surface states due to the dangling bonds at the surface.

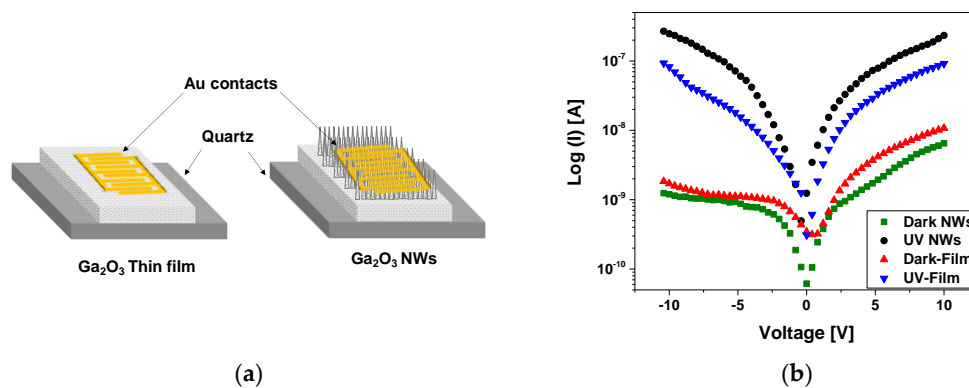


**Figure 13.** (a) Schematic of Au/ $\beta$ -Ga<sub>2</sub>O<sub>3</sub>/Au metal-semiconductor-metal (MSM) photoconductor of  $\beta$ -Ga<sub>2</sub>O<sub>3</sub> thin film (left) and nanowires (right) on quartz. (b) Semi-logarithmic plot of current-voltage for Au/ $\beta$ -Ga<sub>2</sub>O<sub>3</sub>/Au MSM, including  $\beta$ -Ga<sub>2</sub>O<sub>3</sub> thin film and nanowires, versus applied voltage characteristics at 10 V without and with UV illumination at 10 V.

#### 4. Conclusions

A comprehensive study of the effect of silver thin film as an effective catalyst into the growth of Ga<sub>2</sub>O<sub>3</sub> nanostructures was performed. To better understand the role of Ag in the growth dynamics and properties of the Ga<sub>2</sub>O<sub>3</sub> film and nanowires, an Ag-patterned quartz surface was used, which offered the opportunity to investigate concomitantly the growth of gallium oxide on Ag-coated and uncoated surfaces. In this study, different parameters have been explored such as oxidation temperatures, oxygen concentration, oxidation time, and silver thin film thickness. Silver as a catalyst material for the growth of Ga<sub>2</sub>O<sub>3</sub> has shown a great potential for high scale production. Oxygen solubility and diffusivity into silver is high and plays a critical role in enhancing the growth mechanism of Ga<sub>2</sub>O<sub>3</sub>. Our results could offer a simple, low-cost, and promising technique to grow thin film or nanowires for wide optoelectronics and sensing applications.

**Author Contributions:** Conceptualization, B.A.; Methodology, B.A.; Resources, M.S.I.; Data Curation, B.A. and R.B.; Writing—Original Draft Preparation, B.A.; Writing—Review & Editing, B.A., R.B., R.V. and M.S.I.; Supervision, M.S.I.; Project Administration, M.S.I.; Funding Acquisition, M.S.I.

**Funding:** No official grants were received to be reported.

**Acknowledgments:** The author gratefully acknowledged the financial support by Kuwait Institute for Scientific Research.

**Conflicts of Interest:** The authors declare no conflict of interest.

#### References

- Lin, H.-J.; Baltrus, J.P.; Gao, H.; Ding, Y.; Nam, C.-Y.; Ohodnicki, P.; Gao, P.-X. Perovskite Nanoparticle-Sensitized Ga<sub>2</sub>O<sub>3</sub> Nanorod Arrays for CO Detection at High Temperature. *ACS Appl. Mater. Interfaces* **2016**, *8*, 8880–8887. [[CrossRef](#)] [[PubMed](#)]
- Kaya, A.; Mao, H.; Gao, J.; Chopdekar, R.V.; Takamura, Y.; Chowdhury, S.; Islam, M.S. An Investigation of Electrical and Dielectric Parameters of Sol-Gel Process Enabled beta-Ga<sub>2</sub>O<sub>3</sub> as a Gate Dielectric Material. *IEEE Trans. Electron Devices* **2017**, *64*, 2047–2053. [[CrossRef](#)]
- Grillo, A.; Barrat, J.; Galazka, Z.; Passacantando, M.; Giubileo, F.; Iemmo, L.; Luongo, G.; Urban, F.; Dubourdieu, C.; Di Bartolomeo, A. High field-emission current density from  $\beta$ -Ga<sub>2</sub>O<sub>3</sub> nanopillars. *Appl. Phys. Lett.* **2019**, *114*, 193101. [[CrossRef](#)]
- Pearton, S.J.; Yang, J.; Cary, P.H.; Ren, F.; Kim, J.; Tadjer, M.J.; Mastro, M.A. A review of Ga<sub>2</sub>O<sub>3</sub> materials, processing, and devices. *Appl. Phys. Rev.* **2018**, *5*, 011301. [[CrossRef](#)]
- Kaya, A.; Dryden, D.M.; Woodall, J.M.; Islam, M.S. Spontaneous delamination via compressive buckling facilitates large-scale-Ga<sub>2</sub>O<sub>3</sub> thin film transfer from reusable GaAs substrates. *Phys. Status Solidi Appl. Mater. Sci.* **2017**, *214*, 1700102. [[CrossRef](#)]

6. Alhalaili, B.; Mao, H.; Islam, S. Ga<sub>2</sub>O<sub>3</sub> Nanowire Synthesis and Device Applications. In *Novel Nanomaterials—Synthesis and Applications*; Kyzas, G.Z., Mitropoulos, A.C., Eds.; IntechOpen: London, UK, 2017. [[CrossRef](#)]
7. Patil-Chaudhari, D.; Ombaba, M.; Oh, J.Y.; Mao, H.; Montgomery, K.H.; Lange, A.; Mahajan, S.; Woodall, J.M.; Islam, M.S. Solar Blind Photodetectors Enabled by Nanotextured beta-Ga<sub>2</sub>O<sub>3</sub> Films Grown via Oxidation of GaAs Substrates. *IEEE Photonics J.* **2017**, *9*, 1–7. [[CrossRef](#)]
8. Bayam, Y.; Logeeswaran, V.J.; Katzenmeyer, A.M.; Sadeghian, R.B.; Chacon, R.J.; Wong, M.C.; Hunt, C.E.; Motomiya, K.; Jeyadevan, B.; Islam, M.S. Synthesis of Ga<sub>2</sub>O<sub>3</sub> Nanorods with Ultra-Sharp Tips for High-Performance Field Emission Devices. *Sci. Adv. Mater.* **2015**, *7*, 211–218. [[CrossRef](#)]
9. Nguyen, T.D.; Kim, E.T.; Dao, K.A. Ag nanoparticle catalyst based on Ga<sub>2</sub>O<sub>3</sub>/GaAs semiconductor nanowire growth by VLS method. *J. Mater. Sci. Mater. Electron.* **2015**, *26*, 8747–8752. [[CrossRef](#)]
10. Guo, D.; Wu, Z.; Li, P.; Wang, Q.; Lei, M.; Li, L.; Tang, W. Magnetic anisotropy and deep ultraviolet photoresponse characteristics in Ga<sub>2</sub>O<sub>3</sub>: Cr vermicular nanowire thin film nanostructure. *RSC Adv.* **2015**, *5*, 12894–12898. [[CrossRef](#)]
11. Lee, S.Y.; Choi, K.H.; Kang, H.C. Growth mechanism of In-doped beta-Ga<sub>2</sub>O<sub>3</sub> nanowires deposited by radio frequency powder sputtering. *Mater. Lett.* **2016**, *176*, 213–218. [[CrossRef](#)]
12. Choi, K.-H.; Cho, K.-K.; Kim, K.-W.; Cho, G.-B.; Ahn, H.-J.; Nam, T.-H. Catalytic Growth and Structural Characterization of Semiconducting beta-Ga<sub>2</sub>O<sub>3</sub> Nanowires. *J. Nanosci. Nanotechnol.* **2009**, *9*, 3728–3733. [[CrossRef](#)] [[PubMed](#)]
13. Park, S.; Sun, G.J.; Lee, C. UV-assisted room temperature-gas sensing of Ga<sub>2</sub>O<sub>3</sub>-core/ZnO-shell nanowires. *J. Ceram. Process. Res.* **2015**, *16*, 367–371.
14. Jang, Y.-G.; Kim, W.-S.; Kim, D.-H.; Hong, S.-H. Fabrication of Ga<sub>2</sub>O<sub>3</sub>/SnO<sub>2</sub> core-shell nanowires and their ethanol gas sensing properties. *J. Mater. Res.* **2011**, *26*, 2322–2327. [[CrossRef](#)]
15. Ghose, S.; Rahman, S.M.; Arias, A.; Rojas-Ramirez, J. Structural and optical properties of beta-Ga<sub>2</sub>O<sub>3</sub> thin films grown by plasma-assisted molecular beam epitaxy. *J. Vac. Sci. Technol. B* **2016**, *34*, 02L109. [[CrossRef](#)]
16. Feng, Q.; Li, F.; Dai, B.; Jia, Z.; Xie, W.; Xu, T.; Lu, X.; Tao, X.; Zhang, J.; Hao, Y. The properties of gallium oxide thin film grown by pulsed laser deposition. *Appl. Surf. Sci.* **2015**, *359*, 847–852. [[CrossRef](#)]
17. Han, W.; Kohler-Redlich, P.; Ernst, F.; Rühle, M. Growth and microstructure of Ga<sub>2</sub>O<sub>3</sub> nanorods. *Solid State Commun.* **2000**, *115*, 527–529. [[CrossRef](#)]
18. Cao, C.B.; Chen, Z.; An, X.Q.; Zhu, H.S. Growth and field emission properties of cactus-like gallium oxide nanostructures. *J. Phys. Chem. C* **2008**, *112*, 95–98. [[CrossRef](#)]
19. Sharma, S.; Sunkara, M.K. Direct synthesis of gallium oxide tubes, nanowires, and nanopaintbrushes. *J. Am. Chem. Soc.* **2002**, *124*, 12288–12293. [[CrossRef](#)]
20. Pallister, P.J.; Buttera, S.C.; Barry, S.T. Self-seeding gallium oxide nanowire growth by pulsed chemical vapor deposition. *Phys. Status Solidi Appl. Mater. Sci.* **2015**, *212*, 1514–1518. [[CrossRef](#)]
21. Zhao, Y.; Frost, R.L.; Yang, J.; Martens, W.N. Size and morphology control of gallium oxide hydroxide GaO(OH), nano- to micro-sized particles by soft-chemistry route without surfactant. *J. Phys. Chem. C* **2008**, *112*, 3568–3579. [[CrossRef](#)]
22. Reddy, L.S.; Ko, Y.H.; Yu, J.S. Hydrothermal Synthesis and Photocatalytic Property of beta-Ga<sub>2</sub>O<sub>3</sub> Nanorods. *Nanoscale Res. Lett.* **2015**, *10*, 364. [[CrossRef](#)] [[PubMed](#)]
23. Mao, H.; Alhalaili, B.; Kaya, A.; Dryden, D.M.; Woodall, J.M.; Islam, M.S. *Oxidation of GaAs Substrates to Enable β-Ga<sub>2</sub>O<sub>3</sub> Films for Sensors and Optoelectronic Devices (SPIE Optical Engineering + Applications)*; SPIE: San Diego, CA, USA, 2017.
24. Yoshida, T.; Yamamoto, N.; Mizutani, T.; Yamamoto, M.; Ogawa, S.; Yagi, S.; Nameki, H.; Yoshida, H. Synthesis of Ag nanoparticles prepared by a solution plasma method and application as a cocatalyst for photocatalytic reduction of carbon dioxide with water. *Catal. Today* **2018**, *303*, 320–326. [[CrossRef](#)]
25. Arora, K.; Kumar, V.; Kumar, M. Silver plasmonic density tuned polarity switching and anomalous behaviour of high performance self-powered β-gallium oxide solarblind photodetector. *Appl. Phys. Lett.* **2018**, arXiv:1809.10724.
26. omer, V.K.; Malik, R.; Chaudhary, V.; Mishra, Y.K.; Kienle, L.; Ahuja, R.; Lin, L. Superior visible light photocatalysis and low-operating temperature VOCs sensor using cubic Ag(0)-MoS<sub>2</sub> loaded g-CN 3D porous hybrid. *Appl. Mater. Today* **2019**, *16*, 193–203.
27. Tomer, V.K.; Duhan, S. A facile nanocasting synthesis of mesoporous Ag-doped SnO<sub>2</sub> nanostructures with enhanced humidity sensing performance. *Sens. Actuators B Chem.* **2016**, *223*, 750–760. [[CrossRef](#)]

28. Tomer, V.K.; Duhan, S. Ordered mesoporous Ag-doped TiO<sub>2</sub>/SnO<sub>2</sub> nanocomposite based highly sensitive and selective VOC sensors. *J. Mater. Chem. A* **2016**, *4*, 1033–1043. [[CrossRef](#)]
29. Zhao, Y.Y.; Frost, R.L. Raman spectroscopy and characterisation of alpha-gallium oxyhydroxide and beta-gallium oxide nanorods. *J. Raman Spectrosc.* **2008**, *39*, 1494–1501. [[CrossRef](#)]
30. Askeland, D.R.; Fulay, P.P.; Wright, W.J. *The Science and Engineering of Materials*; SI Edition; CL-Engineering: Stamford, CT, USA, 2011; p. 944.
31. Yang, S.M.; Kim, S.R.N.; Youn, W.K.; Kim, C.S.; Kim, D.S.; Yi, K.W.; Hwang, N.M. Generation of Charged Nanoparticles During Thermal Evaporation of Silver at Atmospheric Pressure. *J. Nanosci. Nanotechnol.* **2015**, *15*, 8418–8423. [[CrossRef](#)] [[PubMed](#)]
32. Müller, C.M.; Spolenak, R. Microstructure evolution during dewetting in thin Au films. *Acta Mater.* **2010**, *58*, 6035–6045. [[CrossRef](#)]
33. Strobel, S.; Kirkendall, C.; Chang, J.-B.; Berggren, K.K. Sub-10 nm structures on silicon by thermal dewetting of platinum. *Nanotechnology* **2010**, *21*, 505301. [[CrossRef](#)]
34. Nsimama, P.D. Morphological and Structural Properties of Silver Nanofilms Annealed by RTP in Different Atmospheres. *Am. J. Nano Res. Appl.* **2015**, *3*, 99–104.
35. Lindberg, C.; Whitar, A.; Dick, K.A.; Sköld, N.; Nygård, J.; Bolinsson, J. Silver as Seed-Particle Material for GaAs Nanowires-Dictating Crystal Phase and Growth Direction by Substrate Orientation. *Nano Lett.* **2016**, *16*, 2181–2188. [[CrossRef](#)] [[PubMed](#)]
36. Han, C.Q.; Mao, W.T.; Bao, K.Y.; Xie, H.Q.; Jia, Z.Y.; Ye, L.Q. Preparation of Ag/Ga<sub>2</sub>O<sub>3</sub> nanofibers via electrospinning and enhanced photocatalytic hydrogen evolution. *Int. J. Hydrog. Energy* **2017**, *42*, 19913–19919. [[CrossRef](#)]
37. Zhou, Z.-Y.; Ma, Y.; Han, Q.-F.; Liu, Y.-L. Solubility, permeation, and capturing of impurity oxygen in Au/Ag: A comparative investigation from first-principles. *Comput. Mater. Sci.* **2016**, *114*, 79–85. [[CrossRef](#)]
38. Yasui, K.; Kohiki, S.; Shimooka, H.; Shishido, T. Effects of Au catalyst on growth of beta-Ga<sub>2</sub>O<sub>3</sub> nanostructure at alpha-Al<sub>2</sub>O<sub>3</sub> (0001) surface. *Solid State Sci.* **2008**, *10*, 1860–1863. [[CrossRef](#)]
39. Kim, H.W.; Kim, N.H. Synthesis of beta-Ga<sub>2</sub>O<sub>3</sub> nanowires by an MOCVD approach. *Appl. Phys. Mater. Sci. Process.* **2005**, *81*, 763–765. [[CrossRef](#)]
40. Kumar, S.; Sarau, G.; Tessarek, C.; Bashouti, M.; Hähnel, A.; Christiansen, S.; Singh, R. Study of iron-catalysed growth of beta-Ga<sub>2</sub>O<sub>3</sub> nanowires and their detailed characterization using TEM, Raman and cathodoluminescence techniques. *J. Phys. D Appl. Phys.* **2014**, *47*, 435101. [[CrossRef](#)]
41. Song, P.Y.; Wu, Z.Y.; Shen, X.Y.; Kang, J.Y.; Fang, Z.L.; Zhang, T.Y. Self-consistent growth of single-crystalline ((2)over-bar01)beta-Ga<sub>2</sub>O<sub>3</sub> nanowires using a flexible GaN seed nanocrystal. *CrystEngComm* **2017**, *19*, 625–631. [[CrossRef](#)]
42. Hajakbari, F.; Ensandoust, M. Study of Thermal Annealing Effect on the Properties of Silver Thin Films Prepared by DC Magnetron Sputtering. *Acta Phys. Pol. A* **2016**, *129*, 680–682. [[CrossRef](#)]
43. Zinkevich, M.; Aldinger, F. Thermodynamic assessment of the gallium-oxygen system. *J. Am. Ceram. Soc.* **2004**, *87*, 683–691. [[CrossRef](#)]
44. Tollefson, E.L.; Cambron, A.; Smeltzer, W.W. Adsorption of Oxygen by a Silver Catalyst. *Can. J. Chem. Rev. Can. Chim.* **1956**, *34*, 1046–1060.
45. Zhu, F.; Yang, Z.X.; Zhou, W.M.; Zhang, Y.F. Direct synthesis of beta gallium oxide nanowires, nanobelts, nanosheets and nanograsses by microwave plasma. *Solid State Commun.* **2006**, *137*, 177–181. [[CrossRef](#)]
46. Sajanlal, P.R.; Sreepasad, T.S.; Samal, A.K.; Pradeep, T. Anisotropic nanomaterials: Structure, growth, assembly, and functions. *Nano Rev.* **2011**, *2*, 5883. [[CrossRef](#)] [[PubMed](#)]
47. Shao, D.; Yu, M.; Sun, H.; Hu, T.; Lian, J.; Sawyer, S. High responsivity, fast ultraviolet photodetector fabricated from ZnO nanoparticle-graphene core-shell structures. *Nanoscale* **2013**, *5*, 3664–3667. [[CrossRef](#)] [[PubMed](#)]
48. Weng, W.Y.; Hsueh, T.J.; Chang, S.J.; Huang, G.J.; Hsueh, H.T. A beta-Ga<sub>2</sub>O<sub>3</sub> Solar-Blind Photodetector Prepared by Furnace Oxidization of GaN Thin Film. *IEEE Sens. J.* **2011**, *11*, 999–1003. [[CrossRef](#)]

